Nationaal Lucht- en Ruimtevaartlaboratorium
National Aerospace Laboratory NLR

NLR-TP-2002-415

Design and optimisation of an Ariane 5 LOX line cover

Mode-tracking in B2000

R.J.C. Creemers

Nationaal Lucht- en Ruimtevaartlaboratorium
National Aerospace Laboratory NLR

NLR-TP-2002-415

Design and optimisation of an Ariane 5 LOX line cover

Mode-tracking in B2000

R.J.C. Creemers

This report is based on a presentation held at ECCM-10, Brugge (Belgium), 3-7 June 2002.

Customer:	National Aerospace Laboratory NLR
Working Plan number:	S.1.A.3
Owner:	National Aerospace Laboratory NLR
Division:	Structures and Materials
Distribution:	Unlimited
Classification title:	Unclassified
	August 2002

Summary

In June 2000 a two-year joint programme by Ducth Space, Centre of Lightweight Structures, and the National Aerospace Laboratory NLR was started to develop, manufacture, and qualify a demonstrator fairing (the upper LOX line cover). The aim is a 50 % reduction of the recurring costs of the LOX line cover by design optimisation and the application of a new manufacturing process. In the preliminary design phase the requirements for the Liquid Oxygen (LOX) fairing were investigated. Trade-offs supported by preliminary analyses showed that a CFRP stiffened skin concept in combination with Vacuum Assisted Resin Transfer Moulding (VARTM) technology was the most promising concept in terms of cost reduction, weight reduction and design flexibility. The design optimisation was performed with the B2000 code. Several initial designs, each with a different number of stiffeners, were analysed and optimised, resulting in an optimum design with a 40 % weight and 50 % (recurring) costs reduction.

Keywords: optimisation, composite, fairing, LOX, VARTM

Contents

20 Figures

(32 pages in total)

List of Abbreviations

CFRP	Carbon Fibre Reinforced Plastics
CID	Constraint Identification
CLC	Centre of Lightweight Structures
DUL	Design Ultimate Load
DV	Design Variable
FEM	Finite Element Method
DS	Dutch Space
IDL	Input Description Language
LOX	Liquid Oxygen
MS	Margin of Safety
NIVR	Netherlands Agency for Aerospace Programmes
NLR	National Aerospace Laboratory
OMIDL	Optimisation Model Input Description Language
TP	Thermal Protection
VARTM	Vacuum Assisted Resin Transfer Moulding

List of Symbols

C_{ij}	component i,j in linking matrix
K	global stiffness matrix
$K_{,x}$	global stiffness gradient
k	generalised stiffness
MP^i	i^{th} Model Parameter
m	generalised mass
P	global force vector
$P_{,x}$	global force gradient
TH	Tsai-Hill criterion
U	global displacement vector
$U_{,x}$	global displacement gradient
$\overset{C}{v}_i^j$	eigenvector of mode j in optimisation cycle I
x^j	j^{th} design variable
λ	eigenvalue
σ	normal stress
$\overline{\sigma}$	allowable normal stress
τ	shear stress
$\overline{\tau}$	allowable shear stress

This page is intentionally left blank.

1 Introduction

Ducth Space (DS) is a European supplier of launcher structural systems. DS has been collaborating on the development of the Ariane 5 launch vehicle (see Fig. 1). However, for the traditional expendable launch vehicles, commercial competition is increasing with the associated demand for dramatic cost reductions. Arianespace is looking for a substantial reduction in recurring costs.
A great deal of cost reduction can be achieved by design optimisation. However, it is recognised that additional savings can be realised by the introduction of new manufacturing technologies. A survey on the components and assemblies of the main engine frame of Ariane 5 indicated, that significant savings can be achieved on the fairings over the fuel lines through the introduction of a composite production process. The current fairings are made out of formed, stiffened and riveted aluminium sheet. The manufacturing process is labour intensive and hence costly. DS proposes to replace these metal assemblies by composite components with a high level of part integration. The aim is to reduce the recurring costs by 50 %. Reduction of weight is not a requirement, but the composite fairings should not become heavier than the current metal fairings. Three fairings are covering the Liquid OXygen (LOX) line (see Fig. 2). It was decided to redesign the upper LOX line cover, because it is the most complex of the three fairings.
In June 2000 a two-year joint programme by Dutch Space (DS), Centre of Lightweight Structures (CLC), and the National Aerospace Laboratory NLR was started to develop, manufacture, and qualify the demonstrator fairing. The programme was (partly) sponsored by the Netherlands Agency for Aerospace Programmes (NIVR) within the national NRT programme.

2 Design requirements

2.1 Geometrical requirements

The composite fairing should have the same edge interfaces as the aluminium fairing. Alterations to the outer geometry of the fairing are allowed. However, this has the consequence that a support rig in the lower section of the fairing will have to be redesigned. Further, a stay-out zone at the inside of the fairing has been defined. The deformed/undeformed geometry should not interfere with this zone, because here the LOX line is placed.

2.2 Material requirements

B-basis allowables have to be used for the material properties: the lower limit of the mechanical characteristic corresponds to the value with a 90 % probability of being exceeded, with a 95 % confidence level, according to Jones (1969). Hot/Wet conditions have to be accounted for in the determination of the material properties. Further, there are additional requirements with respect to resistance against certain environmental conditions (like in-flight outgassing), electrical conductivity, air- and watertightness, and compatibility with the Thermal Protection (TP) system.

2.3 Strength requirements

Failure of the structure is not allowed below Design Ultimate Load (1.25 · Limit Load). As stress failure criterion the Tsai-Hill criterion has been chosen:

$$TH = \sqrt{\left(\frac{\sigma_1}{\bar{\sigma}_1}\right)^2 + \left(\frac{\sigma_2}{\bar{\sigma}_2}\right)^2 - \frac{\sigma_1 \cdot \sigma_2}{\bar{\sigma}_1 \cdot \bar{\sigma}_2} + \left(\frac{\tau_{12}}{\bar{\tau}_{12}}\right)^2} \quad . \tag{1}$$

It supposes that there is an interaction between stresses in different directions within a ply. When somewhere in the structure the Tsai-Hill criterion (at DUL) exceeds the value of 1.0, failure occurs. However, for the strength requirement an additional Margin of Safety (MS) of 0.25 has been defined and thus the maximum value for the Tsai-Hill criterion has been set to 0.80.

2.4 Buckling requirements

No global buckling of the structure is allowed below DUL. Local buckling is allowed as long as there is no interference with the stay-out zones. However, in case of local buckling, the structure still has to sustain DUL and the buckling behaviour has to be reversible. To show this, either a test or a non-linear post-buckling analysis has to be performed. As this is a time consuming and thus expensive process, and initial calculations showed that both weight and cost targets will be achieved, it was decided not to allow any buckling (global or local) below DUL. In addition, the MS of 0.25 has to be applied to the buckling requirement as well, so no buckling below 1.25 · DUL.

2.5 Eigenfrequency requirements

The minimum eigenfrequency of the structure is 100 Hz. The eigenfrequency will not be applied as a constraint during optimisation, but after optimisation it will be checked whether it is acceptable. Then the eigenfrequency does not have to be calculated during optimisation, which saves lots of computing effort. For the calculation of the eigenfrequency (after

optimisation) the influence of the thermal protection has to be taken into account. It is assumed that the thermal protection does not contribute to the stiffness (and strength) of the structure. However, the mass of the thermal protection cannot be neglected. The eigenfrequency varies linearly with $\sqrt{k/m}$ where k is the generalised stiffness and m is the generalised mass. As the contribution of the thermal protection to the total mass can be up to 50 %, the eigenfrequency of the structure can be reduced by 30 %.

3 Loads on the LOX line cover

During flight, different mission phases, each with their own loads, can be distinguished:

- Mission phase 1 (ignition): acoustic loads.
- Mission phase 2 (take-off): acoustic loads and blast wave loads.
- Mission phase 3 (atmospheric flight): acoustic loads and aerodynamic loads.

These loads have been converted by DS to static (internal and/or external) pressure loads for the dimensioning of the LOX fairing. The aerodynamic loads depend on the location on the fairing. They are a non-linear function of the X/D-ratio, in which D is the distance between the external face of the fairing and the main stage engine thrust frame, and X is the vertical distance measured down from the top of the fairing (at the top X=0). The dimensioning loads during the optimisation were the combined acoustic and aerodynamic loads during mission phase 3. These pressure loads in three directions (x, y and z). However, simple (hand) calculations showed that the acceleration loads are an order of magnitude smaller than the pressure loads. Therefore, during the optimisation the acceleration loads have been neglected and the combined loads have been applied in a final check only.
In addition to the pressure and acceleration loads, a thermal load has been defined. The peak temperature of the skin under the layer of thermal protection (TP) depends on the design concept (metal/composite/ sandwich structure) and the thickness of the layer of thermal protection. For 6 mm TP the peak temperatures for these structures vary between 146 °C and 151 °C. For safety reasons, a peak temperature of 161 °C is taken.

4 Preliminary design

In the preliminary design phase numerous different design concepts were considered. The two most promising concepts were identified as:

- A CFRP stiffened skin produced by Vacuum Assisted Resin Transfer Moulding (VARTM) or oven curing vacuum prepreg.

- A sandwich construction with CFRP facings and Nomex core produced by oven curing vacuum prepreg.

Trade-offs supported by preliminary analyses showed that both concepts are feasible and that approximately the same amount of cost and weight reduction can be achieved. Therefore, the final choice was made on grounds of design flexibility, technology development and technical risk and it was decided to proceed with the CFRP stiffened skin produced by VARTM. Because of the high operating temperatures of the fairing a resin system with a sufficiently high glass transition temperature T_g (± 185 °C) has been selected. This resin system is relatively expensive, making the total costs of the fairing strongly dependent of the amount of material used (and thus of the structural mass of the fairing).

The current metallic fairing is composed of a prismatic section and a tapered section (see Fig. 3) with outer dimensions of approximately 1.4 x 0.7 x 0.5 m. In the preliminary design it was recognised that the sharp corners in the tapered section are a problem area in terms of stresses and in terms of manufacturing. Therefore, a new geometry has been designed (see Fig. 4) which slightly exceeds the envelope of the metallic fairing. Any influence on the aerodynamic loads is not taken into consideration here.

As stiffener concept, hat-stiffeners were chosen (see Fig. 5). The sides of the stiffeners only contain angle plies (± 45° fabric). Extra longitudinal plies are placed in the top of the stiffener (0°/90° fabric). The skin only contains the 0°/90° fabric. The fabric is a 2x2 Twill, which has an equal amount of tows in warp and weft direction. The 0°-direction is perpendicular to the longitudinal direction of the stiffeners. The minimum height and width of the stiffeners is 20 mm. To have no interference with the LOX line under the cover, the maximum height of the stiffeners is 30 mm. The maximum width is 50 mm. At the edges of the fairing the stiffeners will have to end. To compensate for the loss of bending stiffness, extra 0°/90° plies may be added to the skin. Further, extra ± 45° plies will be added to the skin edges to increase the bearing strength, because the edges are bolted to the main stage engine thrust frame. These extra plies start at the edge of the fairing and run underneath the stiffener to a certain extent. Extra ± 45° plies may be added to the end of the stiffeners as well to create a load path from the top of the stiffeners to the skin.

5 The analysis model

The structure of the LOX line cover is discretised into a FEM analysis model. This has been done manually using the advanced "Input Description Language" (IDL) of the B2000 code, see Merazzi (1995). Using this scripting language it is possible to build the model in substructures. The model is completely parameterised. The parameterisation enables quick changes within the model, such as number of stiffeners, width and height of the stiffeners, lay-up and mesh density

of the LOX fairing. Also loads, boundary conditions and materials are translated into B2000 FEM-format.
The entire model is split up in different files, each file modelling a different part of the structure, i.e., skin prismatic section, stringer prismatic section, skin tapered section, stringer tapered section, etc. These substructures are split up again in sub-substructures, i.e., stringer foot, stringer top, etc. The B2000 input processor handles these files as a kind of subroutines in a computer code. There is a "main programme" which calls all the other components. When a component, i.e. the stringer in the prismatic section, is called in a loop, it is possible to vary the number of stringers.

5.1 Geometry and topology

As mentioned in chapter 3, the acceleration loads will only be applied in a final check. Thus, both structure and loading are symmetric and it is possible to model only half the structure. A FEM model of the configuration with 3 stiffeners in the prismatic section and 2 stiffeners in the tapered section is shown in figure 6. All elements in the FEM model are four-noded Stanley type shell elements. The theory of these elements is described in Stanley (1985).

5.2 Materials

The material properties of the CFRP plies are B-basis allowables, obtained in a test programme. All shell elements are modelled as laminates. Some of these elements have to be given an offset (e.g. the skin beneath the stiffeners). This has been done by using 'air plies', see figure 7 and Arendsen (1998). Air plies are plies with a thickness, but without any significant elastic properties or mass. The thickness of the air plies shifts the effective centre line. This enables for example the shifting of the nodal grid lines, preserving a correct representation of properties leading to correct secondary bending moments. As said before, for the calculation of the eigenfrequency of the structure, the mass of the thermal protection has to be taken into account while the stiffness properties can be neglected. Again plies with a thickness and without any significant elastic properties are added to the laminates. Only now, the plies have mass properties equal to the mass properties of the thermal protection.

5.3 Loading on the LOX fairing

The different load cases are described in chapter 3. Blast wave, acoustic and aerodynamic loads were converted by DS to static pressure loads. These pressure loads have been applied on the elements in the skin as element loads. The non-linear pressure load in the front of the prismatic section has been converted to a constant pressure load for each element using linear interpolation. The magnitude of the pressure load depends on the x-coordinates of the corners of the elements. The B2000 input processor ('b2ip') converts the element pressure loads to nodal forces.

5.4 Boundary conditions

Along the edges the fairing is bolted to the main stage engine thrust frame. The bolted connection is assumed to give simple support to the edges of the fairing. An extra support rig in the tapered section only carries radial and tangential loads.
As both the structure and the loading on the LOX fairing are symmetric, only half the fairing has been modelled and, for the calculation of stresses in the fairing, symmetric boundary conditions have been applied to the nodes in the symmetry plane. For the determination of the eigenfrequency of the structure, calculations have been done both with symmetric boundary conditions and with anti-symmetric boundary conditions to find the mode with the lowest eigenfrequency, which can be symmetric or anti-symmetric.

6 The optimisation model

An analysis model describes the FEM modelling of the structure in terms of nodes, elements, materials, boundaries and loads. An optimisation model describes which (material/geometric) properties may vary, which conditions should be met and how the search for better designs is controlled. The description is done manually, using the advanced "Optimisation Model Input Description Language" (OMIDL) of the B2000 code, see Arendsen (1995). The same kind of structuring of the input decks is used as for the analysis model: a "main programme" controls the input and calls "subroutines".
The changes in design are represented by design variables, like the thickness of the longitudinal plies in the skin. In order to link these variables to the plies of individual elements the so-called linking matrix is used. The optimisation is subject to allowable stress levels, allowable buckling loads and geometric constraints.

6.1 Design variables

The final lay-up of the structure is determined by the optimisation. Therefore the following thicknesses have been defined as design variables:

- Ply thickness of the 0°/90° plies in the skin.
- Ply thickness of the ± 45° plies in the stiffeners.
- Ply thickness of the 0°/90° plies in the top of the stiffeners.
- Ply thickness of the ± 45° angle plies in the end of the stiffeners.
- Ply thickness of the 0°/90° plies in the flat rear part of the fairing.

Further, two geometrical variables have been defined:

- Width of the stiffeners (top).
- Height of the stiffeners.

The angle of the sides of the stiffener with respect to the skin remains constant (60°), so when the top of the stiffener becomes wider, naturally the base becomes wider as well. Notice that the base also becomes wider, when the stiffener becomes higher and the width of the top remains the same.

6.2 Design variable linking

Here a short description of the linking of design variables to FEM details is given. The theoretical background can be found in Arendsen (1994).
The principle of design variable linking is simple: the linking matrix reflects the linear combination of changes in design variables, which results in the change of model details.

$$\left\{MP^{i}_{new} - MP^{i}_{old}\right\} = \left[C_{ij}\right] \cdot \left\{x^{j}_{new} - x^{j}_{old}\right\}. \qquad (2)$$

In this relation MP stands for Model Parameter, x is the Design Variable (DV) and $[C_{ij}]$ is the linking matrix.
For example, DV 6 is called 'width of the stiffeners'. When DV 6 increases, this has to result in a new model with wider stiffeners. The x-coordinates of the nodes in the stiffeners will have to be adapted. The x-coordinate of each node is a Model Parameter and the magnitude of the change is defined in the linking matrix. Notice that when the stiffeners become wider, the skin has to become narrower, so DV 6 is not only linked to the nodal coordinates of the stiffeners, but to the nodal coordinates of the skin as well.

6.3 Constraints

Constraints on the design are stress constraints and buckling constraints. They have been deducted from the design requirements (chapter 2). As stress failure criterion the Tsai-Hill criterion is used. Each ply in each element has to satisfy the Tsai-Hill criterion, but only the outer plies within an element have to be checked and get a Constraint IDentification number (CID 6 and further). Buckling is not allowed below $1.25 \cdot$ DUL. The first four buckling modes are considered during the optimisation and get a CID number of 2-5.
Another type of constraint within B2000 is the objective itself (CID 1). The objective is the structural mass of the entire LOX fairing, because the total costs are strongly related to the mass.

7 The optimisation procedure

Several configurations of the fairing were analysed and optimised. To achieve a fully optimised design the following optimisation process has to be used:

1. Build analysis model with initial geometry and thicknesses ('b2ip')
2. Build optimisation model with initial geometry and thicknesses ('b2omip')
3. Run/continue optimisation ('b2opt') while calculating the amount of change of the base of the stiffener:

$$\frac{\left|\text{base}_{\text{new}} - \text{base}_{\text{ini}}\right|}{\text{base}_{\text{ini}}} < 0.15 ?$$

   - No: return to 1. using the results of the optimisation for the initial geometry and thicknesses
   - Yes: goto 4.
4. Convergence?
   - No: return to 3.
   - Yes: stop

This method has to be used because of the following. The structure is in a state of static equilibrium:

$$K \cdot U = P \tag{3}$$

where K is the global stiffness matrix, U the global displacement vector and P the global force vector. As said before, the pressure distribution is converted to nodal loads by the input processor. Then, the change of geometry causes a non-uniform pressure distribution on the LOX fairing (illustrated in Fig. 8), which in reality is not the case. The vector containing the nodal loads is no longer correct. Further, the optimisation uses the derivative of equation (3) with respect to the Design Variable to calculate the displacement/stress gradients in each optimisation step (Maxi-cycle) for the determination of search directions:

$$K_{,x} \cdot U + K \cdot U_{,x} = P_{,x} . \tag{4}$$

Usually the right hand term in equation (4) can be neglected ($P_{,x} = 0$), but clearly, this is not allowed here. The nodal forces depend on the geometrical variables (stiffener width and height) and therefore $P_{,x} \neq 0$.

When the optimisation is restarted with the changed geometry as initial geometry, the nodal forces are recalculated for the uniform pressure distribution and therefore are correct again. Figure 9 shows the influence of neglecting the changed nodal loads on the optimisation (without restart) for the configuration with 4 stiffeners in the prismatic section and 2 stiffeners in the tapered section. Maxi-cycle 1 to 4 all represent infeasible designs. The first feasible design is found at Maxi-cycle 5. Here, the geometrical design variables both reached their maximum values and the above-discussed effect (non-uniform distribution of the pressure) is relatively large. The optimisation without the restart finds an optimum that is close to the first feasible design. In the modified procedure, the base of the stiffener changed more than 15 % with respect to the initial design in Maxi-cycle 2 and 4, so here the optimisation was restarted. The results of this modified procedure are shown in figure 9 as well. As can be seen the optimisation converges faster and it results in a design with a much lower weight. Although the procedure does not take into account the change of the nodal forces at each step, it is comparable to an optimisation procedure which does modify the nodal forces at each step, because when the change of the pressure distribution becomes too large (e.g. 15 %) due to the change of the geometrical variables, the nodal forces are recalculated and the pressure distribution is uniform again. In this chapter it is shown clearly that an optimisation without restarts may find the wrong optimum, but even with restarts one has to be very careful when to restart the optimisation.
Of course there are other ways (than restarting the optimisation) to solve the problem. The change of nodal forces could be solved by linking the geometrical design variables to the nodal forces, but ideally this problem would be solved by the optimisation itself by no longer neglecting the change of nodal forces. This will give a result similar to the modified procedure but without restarting the optimisation. This feature has been programmed into the development code of B2000 (in the input processor 'opip'). The processor is operational, but it has not been tested extensively yet.

8 The optimisation results

Several fairing configurations have been optimised. The results showed that the configuration with 4 stiffeners in the prismatic section and 3 stiffeners in the tapered section has the lowest weight. The optimisation results of the 4-3 configuration will be discussed here in greater detail. For the optimisation of the 4-3 configuration of the LOX fairing, the optimisation procedure, discussed in the previous chapter, was used. As restart criterion a change of 10% of the base of the stiffener was chosen and the optimisation had to be restarted in Maxi-cycle 2, 5, 7 and 13. The history results of the optimisation can be seen in figures 10 to 13. In these figures ply thicknesses, width and height of the stiffeners, structural weight, and certain relevant constraints

of the LOX fairing are shown for each optimisation cycle. The definition of a constraint within B2000 is such, that a positive constraint value indicates a violated constraint (and thus the design is infeasible). In figure 13 it can be seen that the initial design is an infeasible design. Several stress constraints are violated. This is shown in figure 14 as well. Here the Tsai-Hill criterion in each element of the fairing is plotted. As can be seen there are several grey areas. These are the areas with a Tsai-Hill criterion larger than 0.8, the allowable value.
The optimisation starts with a search for a feasible design (with a constraint violation minimisation). At Maxi-cycle 3 the first feasible design has been found, while the weight has increased from 5.03 kg to 7.57 kg. From here the optimisation continues with an objective function (weight) optimisation, resulting in an optimised design. The weight of the design decreases to 6.30 kg. Several stress constraints are critical for the optimised design. The Tsai-Hill criterion in each element of the optimised design is shown in figure 15. Several parts of the fairing have reached the allowable value of 0.80 for the Tsai-Hill criterion:

- The top of the stringer in the prismatic section (at the corners in the curved part).
- The end of the stringer in the prismatic section (at the stringer foot).
- The flat rear part of the fairing (at the corner).

Buckling is critical as well. The first eigenmode is found at an eigenvalue of $\lambda = 1.25$, so at a buckling load of $1.25 \cdot$ DUL.
As can be seen in the optimisation history, the process has great difficulties with converging between cycles 8 and 13. The phenomenon causing this will be discussed here. The optimisation history shows a large variation of the constraint values that correspond to buckling of the structure. In general, the buckling constraints vary highly non-linear with the Design Variable (e.g. buckling of the skin between the stiffeners depends on the thickness of the skin to the power three and the distance between the stiffeners to the power two). Therefore, it is important that the second order derivatives of the buckling constraints with respect to the DV's are correct. For the calculation of the second order derivative, the first order derivatives of two consecutive optimisation cycles are used. However, the first buckling constraint (CID 2) corresponds to the buckling mode with the smallest eigen*value* (and therefore largest constraint value), but it does not correspond to a particular buckling *mode*. Therefore, from one optimisation cycle to another these buckling modes can exchange CID's (hereafter referred to as mode jumping). The second buckling mode (CID 3) in the first cycle might get the smallest eigenvalue in the second cycle due to the changing geometry and thicknesses and therefore it will become the first buckling mode (CID 2) in the second cycle. Now, when the second order derivative of CID 2 is determined, the first order derivatives of two non-equal buckling modes in the two consecutive optimisation cycles are used. Then, the results for the second order derivative will not be correct, thereby misguiding the optimisation. A detailed view of the first three buckling constraints (CID 2, 3 and 4) and buckling modes shows that mode-jumping repeatedly occurred during cycles 8 and 13. The three modes involved are shown in figures 16 to 18. The constraint

values corresponding to a particular mode shape are plotted in figure 19. It can be seen that mode shape 3 in cycle 9 (CID 4) gets the smallest eigenvalue (and largest constraint value) in cycle 10 and therefore gets CID 2. Further, mode shape 1 gets CID 3, and mode shape 2 gets CID 4. Therefore, the second order derivatives of the constraints will not be correct. To get correct second order derivatives for each CID, mode tracking would have to be incorporated in the optimisation. Only recently, this has been programmed in the development code of B2000 and the first results with test cases show a much smoother behaviour of the DV's when mode-jumps occur, but mode tracking is incorporated. This is shown in chapter 9. For the optimisation of the LOX fairing a different method has been used. Starting from cycle 13, the relative variations of the DV's are allowed to be only small (5 % in stead of 10 %). Then, for the optimisation a correct second order derivative is less important compared to the first order derivative, and a relatively quick convergence is the result, see figures 10 to 13.

9 Mode-tracking in B2000

As shown in the previous chapter, mode jumping during optimisation may cause bad convergence of the optimisation process when no mode-tracking is incorporated. The mode jumps cause an error in the calculation of the second order derivatives of the buckling/eigenfrequency constraints with respect to the design variables. Therefore, mode-tracking has been incorporated in order to use the first order derivatives of a certain mode *shape* in the calculation instead of the first order derivatives belonging to certain CID number.
In the buckling/eigenfrequency calculations the eigenvectors of each mode are determined. The eigenvector of a certain mode is always perpendicular to the eigenvector of any other mode. Then, the scalar product of the eigenvector of a certain mode with the eigenvector of any other mode will be equal to zero, but also, the scalar product of the eigenvector of a certain mode with itself will be non-zero. This feature is used to find similar mode shapes in two consecutive cycles. The scalar product is calculated for the eigenvector of mode 'j' in optimisation cycle 'i' with the eigenvector of mode 'k' in optimisation cycle 'i-1' (the previous optimisation cycle):

$$\mathrm{scpr}_{i,j,k} = \frac{\vec{v}_i^{\,j} \cdot \vec{v}_{i-1}^{\,k}}{\left|\vec{v}_i^{\,j}\right|} \tag{5}$$

in which scpr is the normalised result of the scalar product. When the result of the scalar product is zero (or close to zero) the mode 'j' in the current cycle is not similar to mode 'k' in the previous cycle, when the result is one (or close to one) two similar modes have been found. Using this, for each mode in the current cycle, the similar mode in the previous cycle can be

found. For instance, buckling mode 1 in cycle 5 is similar to buckling mode 3 in cycle 4 (the previous cycle) when the normalised result of the scalar product for the eigenvector of mode 1 in cycle 5 ($\vec{v}_5^1$) with mode 3 in cycle 4 ($\vec{v}_4^3$) is (close to) one. As a consequence, the normalised result of the scalar product for the eigenvector of mode 1 in cycle 5 with any other mode in cycle 4 will be close to zero, as these modes cannot be similar as well. When no similar modes in the previous cycle can be found for a certain mode, apparently a new mode has been found. Due to the changing geometry or thickness of the structure a mode appears in the current cycle, which was not present in the structure in the previous cycle.
The optimisation process has been adapted such, that in each cycle a list is generated which contains for each mode the corresponding mode in the previous cycle. For instance:

```
Data set "BMODOR.LACY.10.0.1", idiv      0, type "I   ", size       10
  print from       1 to      10 step       1

    1    3    2    4   -1    6    5   -2    7    8
```

In the data set ‘BMODOR.LACY.10.0.1’, for cycle 10 and load case 1, the corresponding buckling modes in the previous or last cycle are listed. The data set shows that buckling mode 1 in the current cycle (cycle 10) corresponds with buckling mode 1 in the last cycle (cycle 9). Buckling mode 2 in cycle 10 corresponds to buckling mode 3 in cycle 9, buckling mode 3 in cycle 10 corresponds to buckling mode 2 in cycle 9, etc. When a new mode is found, this is indicated by a negative number; e.g. -1 on place five in the list means that the fifth mode in cycle 10 is the first buckling mode for which no similar mode in cycle 9 could be found; it is the first new mode in cycle 10. Similarly, -2 on place 8 means that the eighth mode in cycle 10 is the second buckling mode for which no similar mode in cycle 9 could be found; it is the second new buckling mode.
For certain buckling modes, a constraint has been specified. With the buckling mode list the corresponding (or reference) mode in the previous cycle can be identified. Next, the CID number of the reference mode can be determined, which (as said before) is not necessarily equal to the CID number of the buckling mode in the current cycle. For instance, CID 102 defines a constraint on the second buckling mode and CID 103 defines a similar constraint on the third buckling mode. For the calculation of the second order derivative for CID 102 in cycle 10, the first order derivative for CID 102 in cycle 10 is used together with the first order derivative for CID 103 in cycle 9, because CID 102 in the current cycle corresponds to buckling mode 2 in the current cycle, but to buckling mode 3 (or CID 103) in the last cycle, as was shown in the data set ‘BMODOR.LACY.10.0.1’. It is possible that for the reference mode no constraint was specified, for instance because the reference mode is a new mode. Then, there is no CID for the referenced mode, and therefore, no constraint value or first order derivative has been determined in the last cycle. In that case, the second order derivative is set to zero. In most cases this will be

better than calculating the second order derivative with a wrong first order derivative in the last cycle, as was the case before mode-tracking was incorporated. The results of a test case are shown in figure 20. It can be seen that the new optimisation process converges much smoother (and faster) to its optimum. The test case is a stringer stiffened panel with three design variables (thickness of skin, thickness of blade stiffener, and height of blade stiffener) with constraints on the first 5 buckling loads. Mode jumps occurred often during the optimisation and it can be seen clearly that this redirects the old optimisation without mode-tracking in the wrong direction. See for instance cycle 9. Due to a mode jump from cycle 8 to 9, the wrong second order derivative is calculated for a certain buckling constraint. This wrong second order derivative misguides the optimisation and the resulting change of the design variables is clearly not the best one. It can be concluded that the extension of the optimisation code with mode-tracking can be very beneficial for the convergence of the optimisation.

10 The final design

The optimisation results are translated to a final design by rounding up or down the ply thicknesses to a discrete number of plies and by reviewing the stiffener geometry. On this design a stress analysis (with the combined pressure and acceleration loads), a buckling analysis and an eigenfrequency analysis has been performed, showing that all requirements are satisfied. Further, the final design of the composite LOX fairing offers a structural weight reduction of approximately 40 % with respect to the aluminium design, which would probably be less, if the aluminium was optimised as well. The non-structural weight of the thermal protection is approximately equal for the metallic and composite fairing. Calculations (involving the amount of material, labour, etc.) performed by CLC show that the aim of a 50 % (recurring) cost reduction will be achieved, which is mainly caused by the new design concept (CFRP stiffened skin by VARTEM with a high level of part integration).

11 Conclusions

Material properties were determined in a test programme. These properties are B-basis allowables and they have been used in the FEM calculations. A finite element analysis and optimisation model of the upper LOX line cover has been built in the finite element code B2000, using the results of the preliminary design phase (design concept, geometry, lay-up) as initial design. By using the "Input Description Language" and the "Optimisation Model Input Description Language" the model has been completely parameterised and this enabled the quick changes of number of (hat-) stiffeners, lay-up, mesh density, etc.

Several configurations, each with a different number of stiffeners, have been analysed and optimised. The fairing configuration with four stiffeners in the prismatic section and three stiffeners in the tapered section is the design with the lowest (on which the costs strongly depend due to the expensive matrix material with its high glass transition temperature. Further, it has been shown that incorporating mode-tracking into the optimisation may enhance the convergence of the optimisation significantly when mode-jumping occurs.
The optimised design has been translated to a final design by rounding up or down the ply thicknesses to a discrete number of plies and by reviewing the geometry. An analysis has shown that the final design meets all technical requirements and offers a significant (structural) weight reduction of approximately 40 % compared to the current metallic fairing. The weight of the non-structural thermal protection is approximately equal for both fairings. Calculations (involving the amount of material, labour, etc.) performed by CLC show that the aim of a 50 % recurring cost reduction will be achieved. This design will be further detailed resulting in the issue of production drawings of a mould and of a full scale fairing demonstrator.

12 References

1. Arendsen, P.; *The B2000 Optimization Module: B2OPT*, Amsterdam, National Aerospace Laboratory NLR, NLR-TP-94116, 1994.
2. Arendsen, P.; *B2OPT Processors and Input Description*, Amsterdam, National Aerospace Laboratory NLR, NLR-CR-95179, 1995.
3. Arendsen, P.; *Optimization Study of the Window Area for an Ultra High Capacity Aircraft*, Amsterdam, National Aerospace Laboratory NLR, NLR-TR-98422, 1998.
4. Jones, B.H.; *Determination of Design Allowables for Composite Materials*, American Society for Testing and Materials, ASTM STP 460, 1969.
5. Merazzi, S.; *B2000 Input Description Language (IDL)*, Bienne, Switzerland, SMR Corp, 1995.
6. Stanley, G.M.; *Continuum Based Shell Elements*, Lockheed Applied Mechanics Laboratory, 1985.

Fig. 1 The Ariane 5 launch vehicle

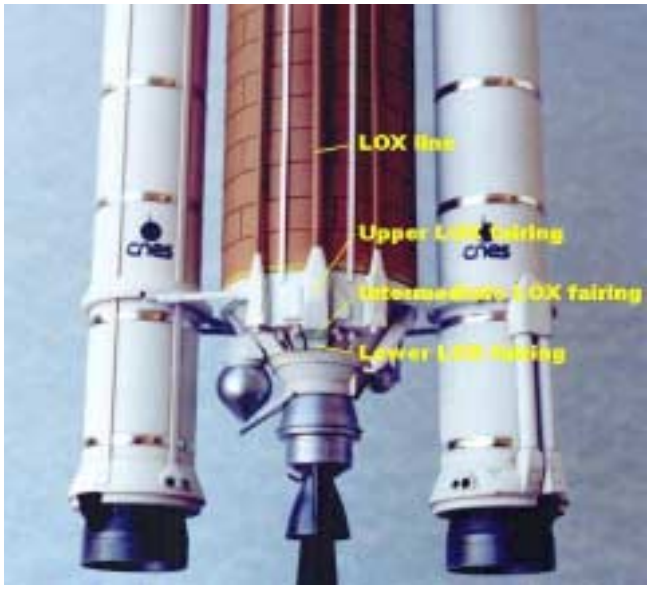

Fig. 2 The covers over the LOX line of Ariane 5

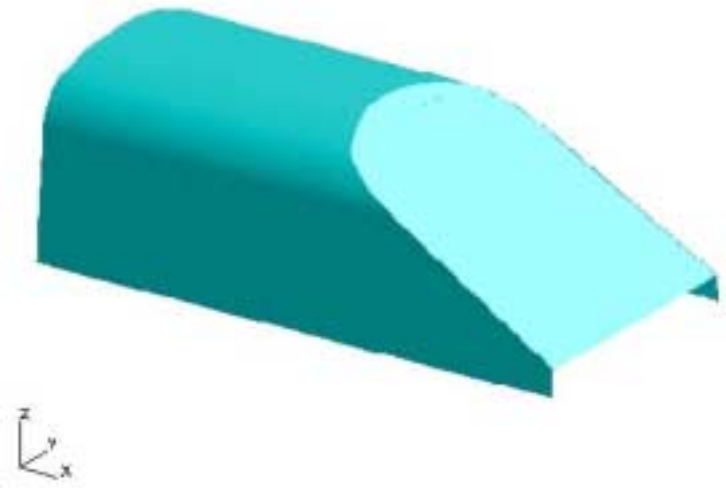

Fig. 3 The outer geometry of the current fairing

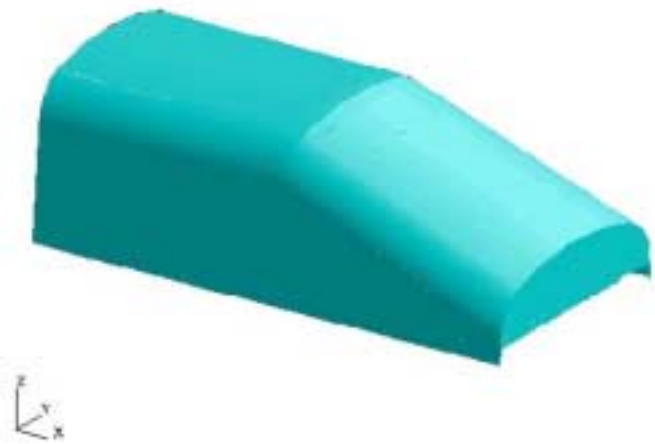

Fig. 4 The outer geometry of the composite fairing

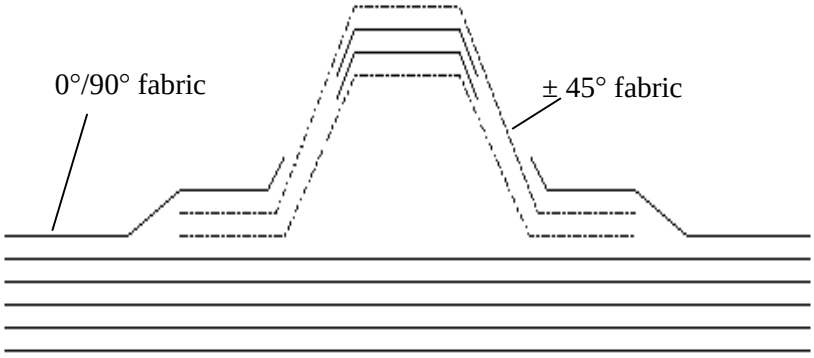

Fig. 5 The hat-stiffener concept

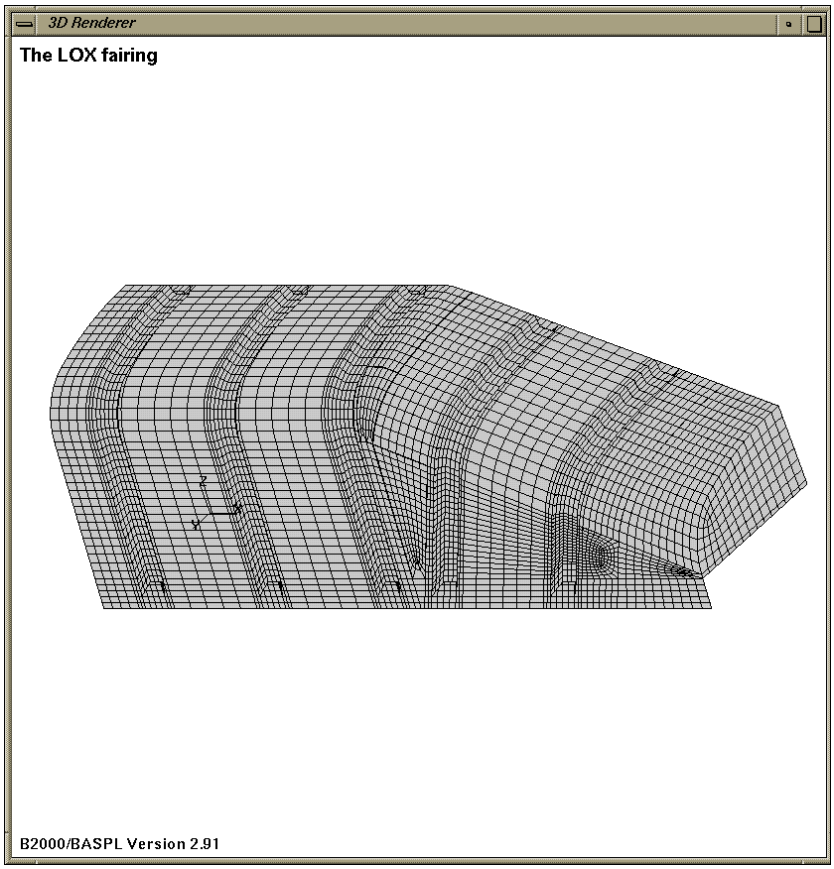

Fig. 6 FEM model of the LOX fairing (3-2 config)

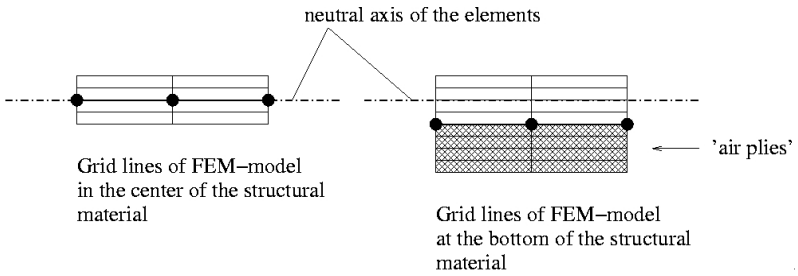

Fig. 7 The usage of air plies in the FEM model

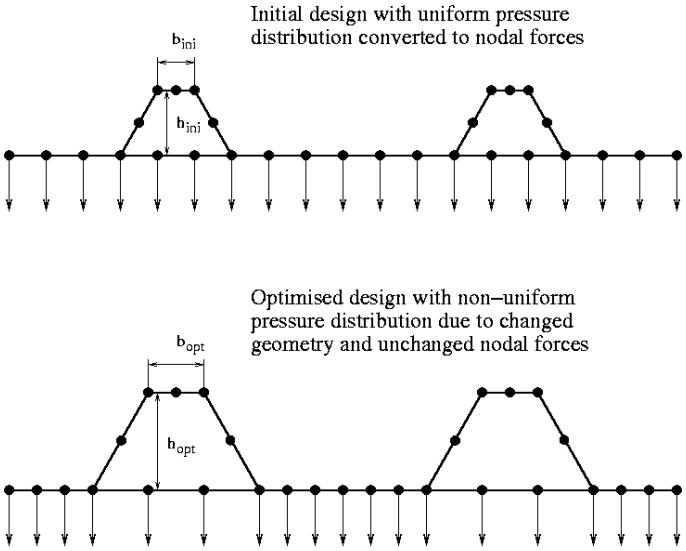

Fig. 8 The nodal loads on the LOX fairing

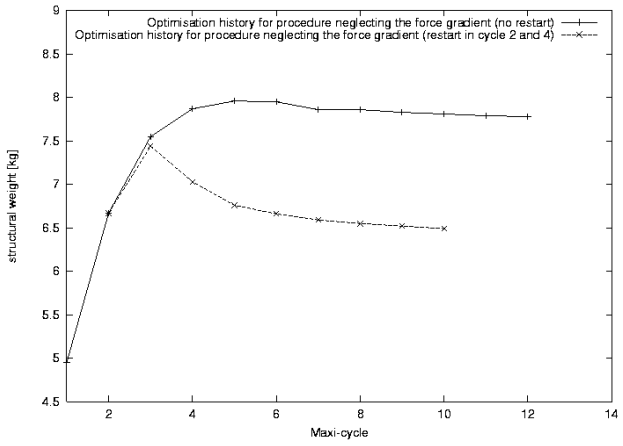

Fig. 9 The optimisation history for the 4-2 config.

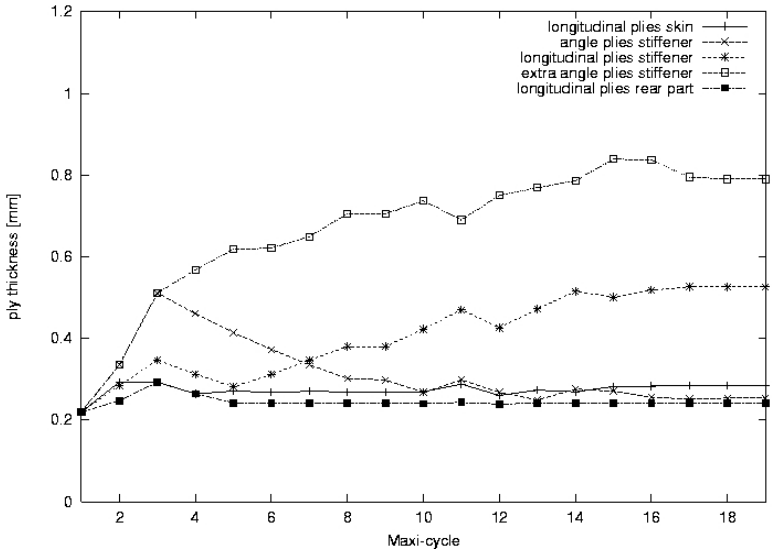

Fig. 10 Ply thicknesses for the 4-3 config. during optimisation

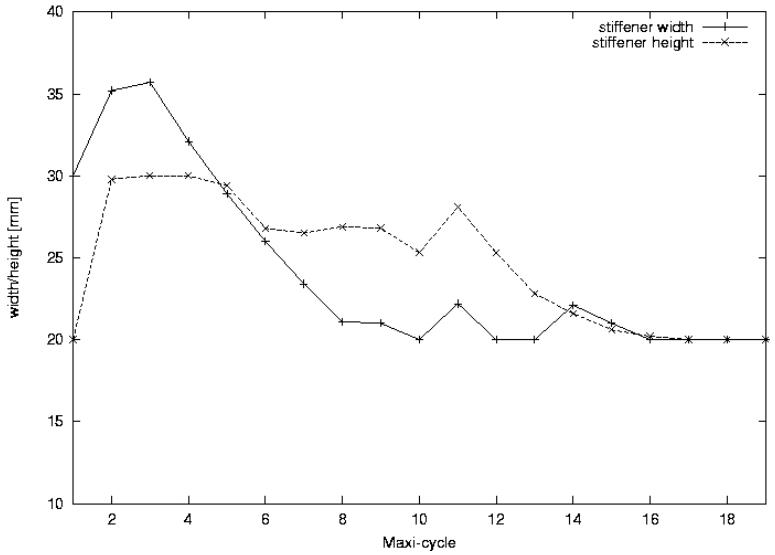

Fig. 11 Stiffener width/height for the 4-3 config. during optimisation

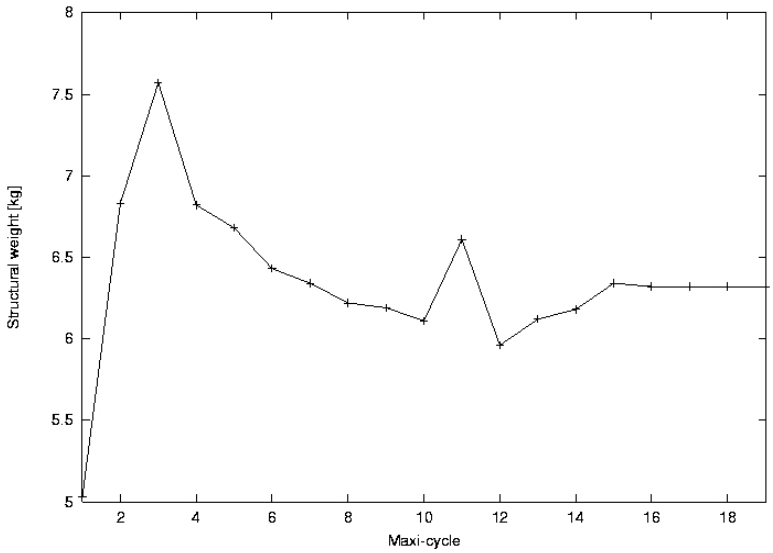

Fig. 12 Structural weight for the 4-3 config. during optimisation

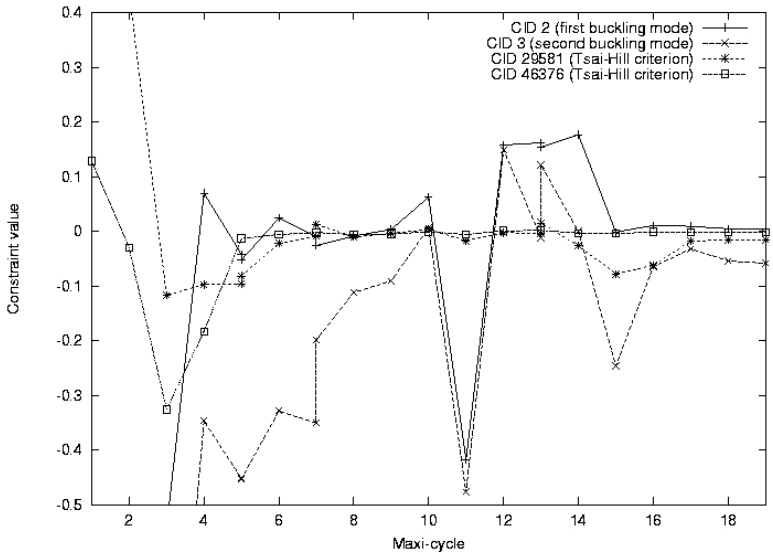

Fig. 13 Constraint values for the 4-3 config. during optimisation

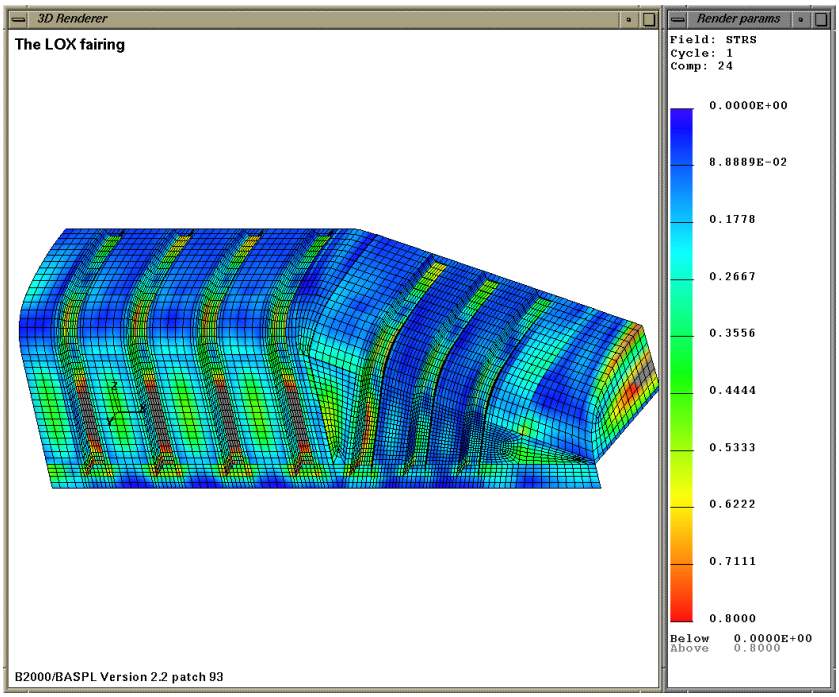

Fig. 14 TH-criterion in the fairing, initial design

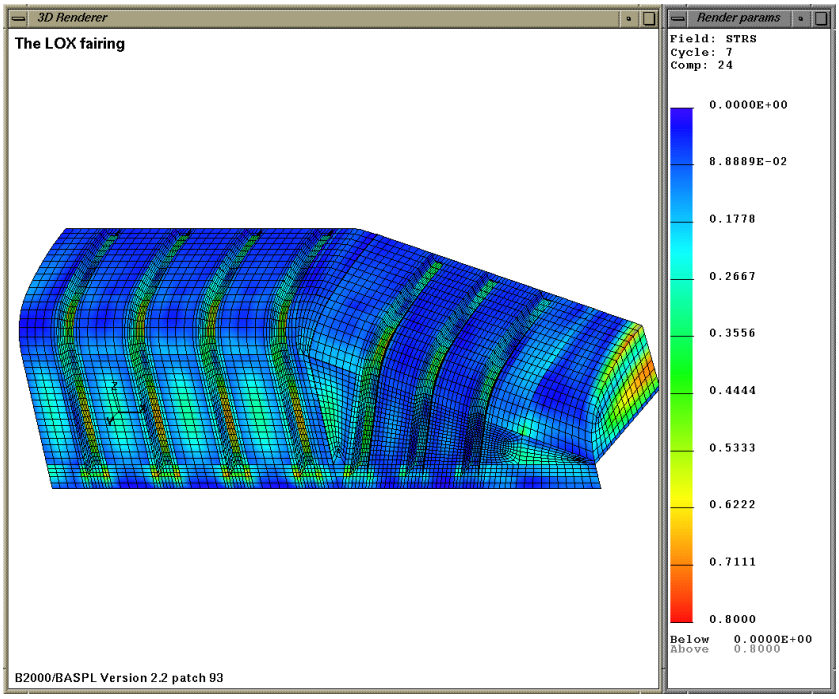

Fig. 15 TH-criterion in the fairing, optimised design

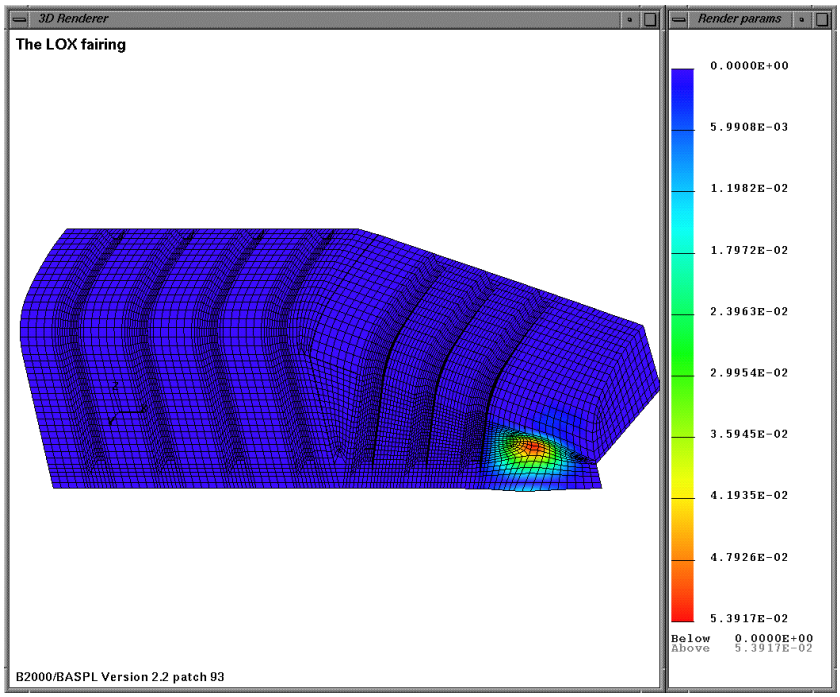

Fig. 16 Mode shape 1: skin buckling lower section

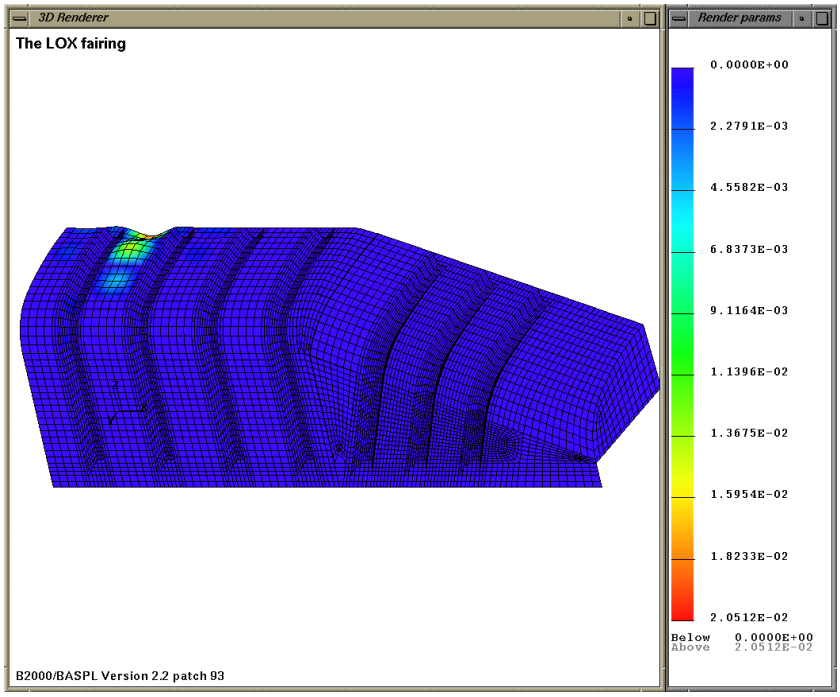

Fig. 17 Mode shape 2: skin buckling upper section

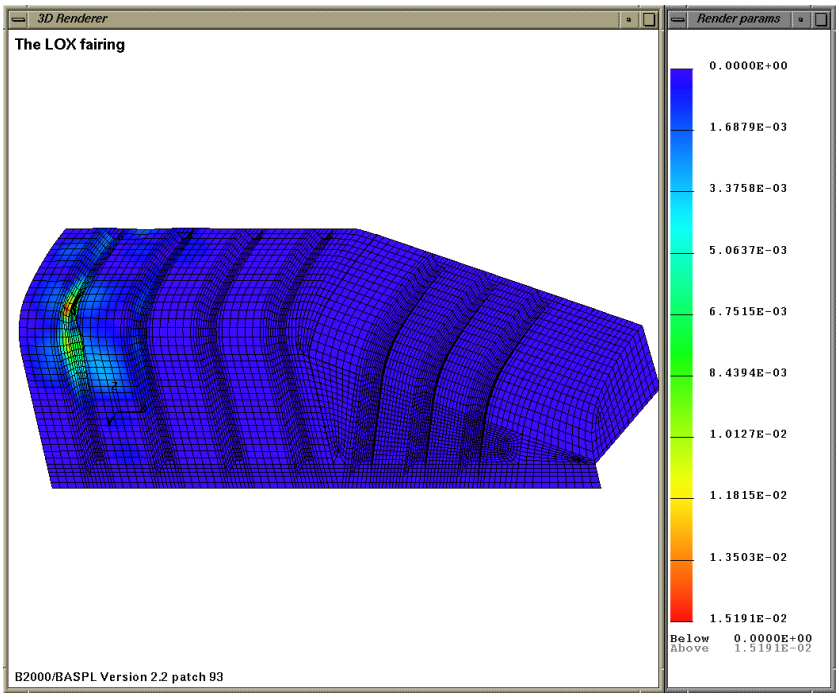

Fig. 18 Mode shape 3: stiffener buckling

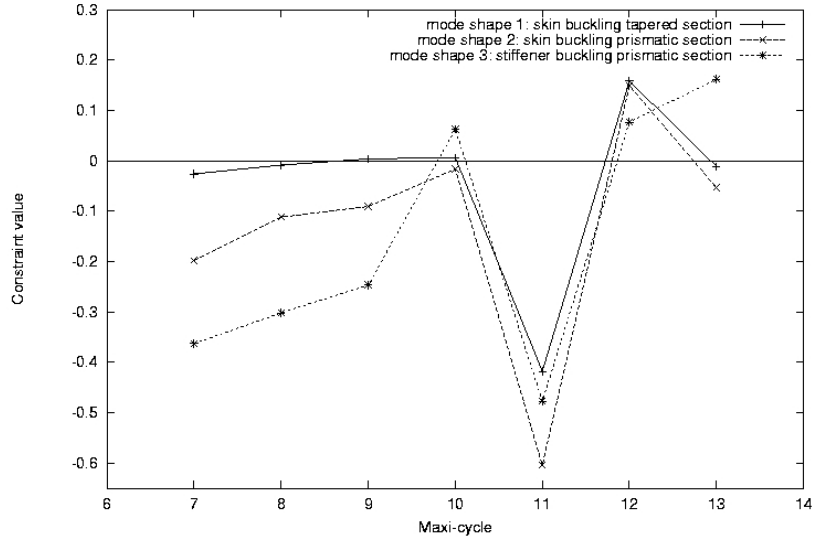

Fig. 19 Constraint values of the buckling modes

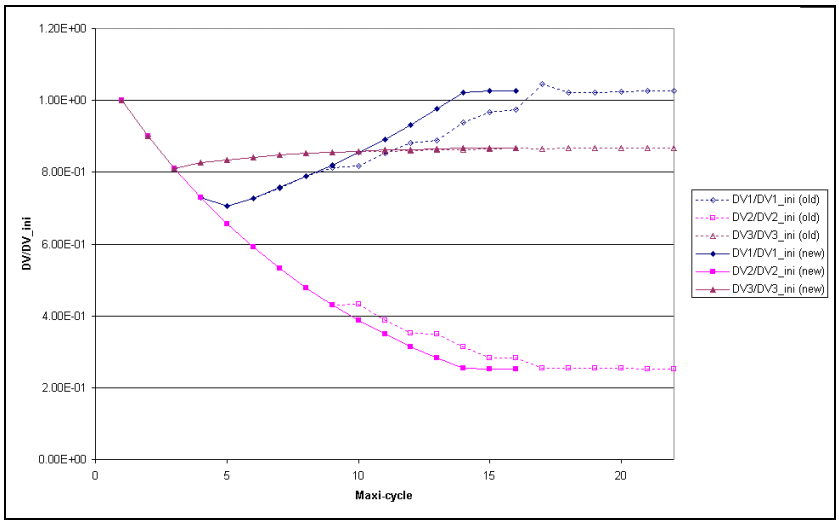

Fig. 20 Optimisation history for a test case with/without mode-tracking